JOC The Journal of Organic Chemistry

pubs.acs.org/joc Article

Tunable Artificial Enzyme–Cofactor Complex for Selective Hydrolysis of Acetals

Ishani Bose, Shixin Fa, and Yan Zhao*

Cite This: J. Org. Chem. 2021, 86, 1701–1711 Read Online

ABSTRACT: Enzymes frequently use unimpressive functional groups such as weak carboxylic acids for efficient, highly selective catalysis including hydrolysis of acetals and even amides. Much stronger acids generally have to be used for such purposes in synthetic systems. We report here a method to position an acidic group near the acetal oxygen of 2-(4-nitrophenyl)-1,3-dioxolane bound by an artificial enzyme. The hydrolytic activity of the resulting artificial enzyme–cofactor complex was tuned by the number and depth of the active site as well as the hydrophobicity and acidity of the cofactor. The selectivity of the complex was controlled by the size and shape of the active site and enabled less reactive acetals to be hydrolyzed over more reactive ones.

INTRODUCTION

Enzymes are fascinating catalysts from nearly every perspective.[1] They catalyze some of the most challenging reactions in nature with astounding efficiency under mild conditions. They possess exquisite selectivity, which are able to pick a particular substrate to react when numerous other ones are present in the same mixture. Even more amazing is that they use "unimpressive" functional groups to accomplish these extraordinary tasks. Serine protease, as an example, relies on a serine–histidine–aspartic acid catalytic triad to hydrolyze amide bonds that would otherwise require concentrated hydroxide or strong acids at elevated temperatures.[2] Both aspartic protease[3] and glycosidase[4,5] have a pair of carboxylic acids in their active sites for the hydrolysis of amides and acetals (in glycosides), respectively.

Central to the catalytic performance of an enzyme is its molecular recognition. When only the substrate can enter the catalytic active site or induce the necessary conformational change to turn on catalysis, other structural analogues will stay intact even if they have the same reactive group as the substrate. In recent years, increasing attention has been paid toward synthetic catalysts with similar molecular recognition features. Some exciting developments emerged from these studies, including selective activation of the C–H bond,[6] Diels–Alder reaction at unreactive sites of anthracene,[7] acidic catalysis under basic conditions,[8] and phosphorylation of a particular hydroxyl among numerous others with similar reactivity.[9] Despite the tremendous progress made, however, these enzyme mimics are rather rudimentary compared to their natural counterparts and construction of multifunctionalized active sites with accurately positioned catalytic groups remains difficult.

Our group has been interested in creating enzyme-mimetic catalysts using different platforms including foldamers and cross-linked micelles/reverse micelles.[10−13] More recently, we developed a method to perform molecular imprinting[14,15] in surface–core doubly cross-linked micelles.[16] Molecular imprinting is a powerful technique to construct guest-tailored binding sites through templated polymerization. Molecularly imprinted polymers are useful in many applications including catalysis.[17−30] When performed in the nanospace of a micelle, molecular imprinting yields receptors capable of distinguishing the shift of a single methyl group or addition/deletion of a single methylene in the guest.[31] These so-called molecularly imprinted nanoparticles (MINPs) resemble enzymes in their water solubility, the nanodimension, and a hydrophilic/hydrophobic surface/core morphology. Complex biomolecules including oligosaccharides[32,33] and peptides[34] can be used as templates with appropriate functional monomers included in the MINP preparation.

In this paper, we report an MINP-based artificial enzyme–cofactor complex for selective hydrolysis of acetals. The MINP was able to bind both the substrate and the acid catalyst in its imprinted site and help position the acidic group near the acetal oxygen of the substrate. Close proximity of the reactive group and the catalytic group allowed weak carboxylic acids to work as well as much stronger sulfonic acids in certain

Received: October 22, 2020
Published: January 5, 2021

https://dx.doi.org/10.1021/acs.joc.0c02519
J. Org. Chem. 2021, 86, 1701–1711

Scheme 1. Preparation of Noncovalent MINP with a Schematic Representation of the Cross-Linked Structure

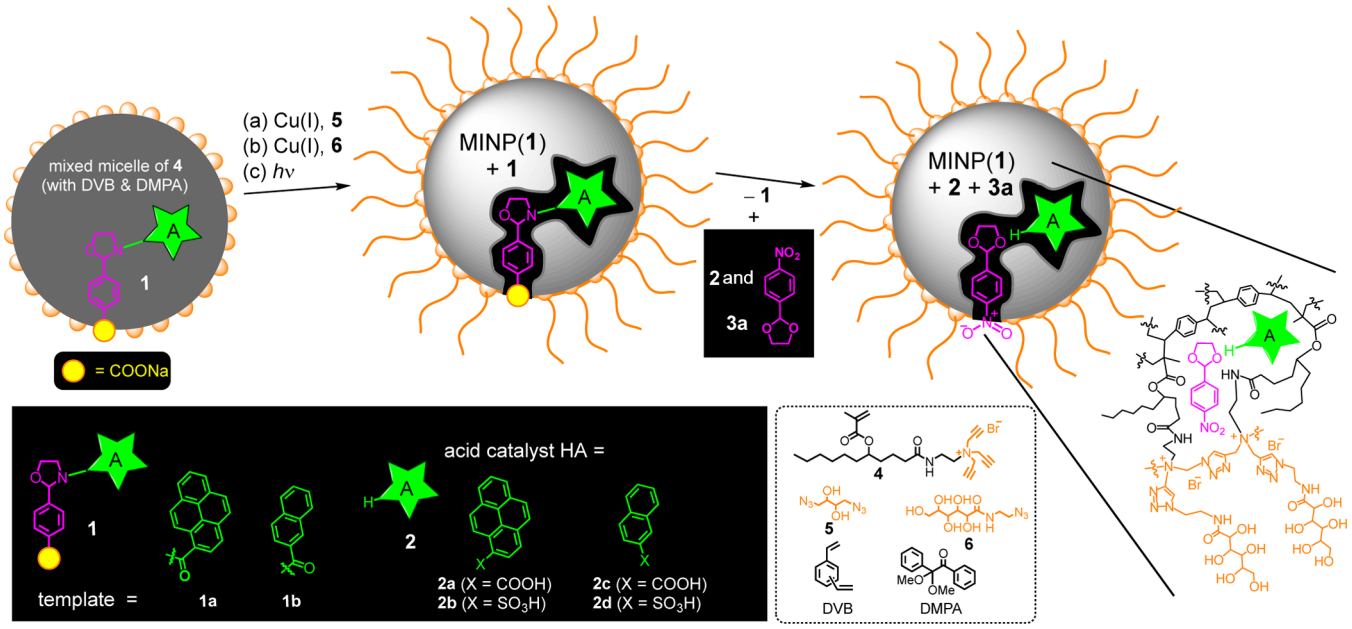

Scheme 2. Synthesis of Compounds 1a–d

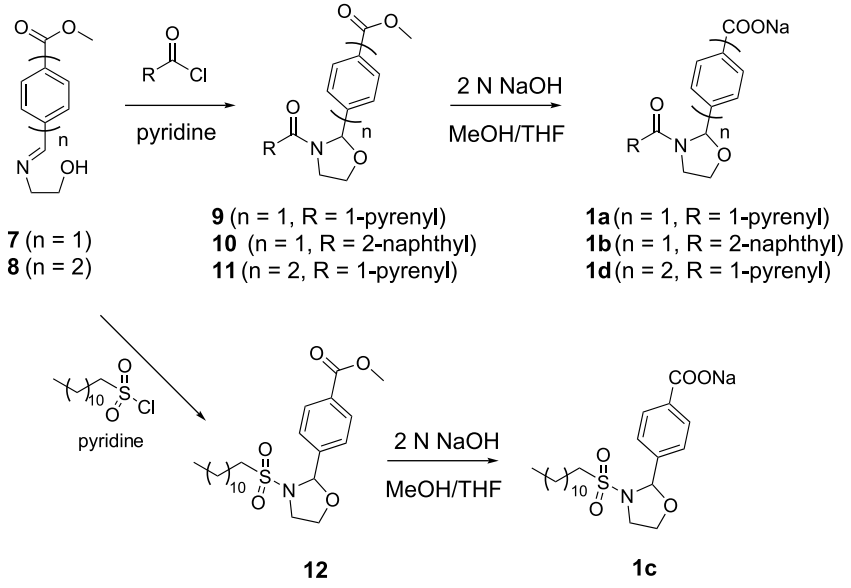

constructs. A key feature of the system is the facile tuning of catalytic activity by easy "plug-and-play" switching of the acid cofactor, which could not be achieved if the acid groups are covalently attached to the active site.[35] In addition, both the number of acid cofactors and the depth of the active site impacted the catalysis strongly. The artificial enzyme–cofactor complex was able to distinguish subtle structural features of the substrates and even hydrolyze less reactive acetals over more reactive ones—a feature frequently seen in enzymatic catalysis but rare in chemical catalysis.

RESULTS AND DISCUSSION

Design and Synthesis of MINP Catalysts. To make weakly acidic carboxylic acids into effective catalysts, enzymes have to position the acids in close proximity to the reactive functionality. Our strategy to enforce such a spatial relationship was to imprint a construct with a substratelike and a catalyst-like moiety (Scheme 1). Template **1** is color-coded to illustrate the purpose of its different substructures: the green moiety is the space holder for a noncovalently bound catalyst **2**, the magenta resembles the substrate 2-(4-nitrophenyl)-1,3-dioxolane (**3a**), and the yellow is for the carboxylate group that serves as a hydrophilic anchor. The *para*-nitro-substituted acetal was chosen for its low background activity. The anionic anchor was used to keep the template molecule and, in turn, the imprinted site close to the surface of the micelle. Such a location is expected to facilitate the removal of the template after imprinting and also make the imprinted site readily accessible to the substrate during the catalysis. If a binding site could be faithfully imprinted from the template, the MINP would be able to bring substrate **3a** and acid catalysts (**2a–d**) together in a way similar to what an enzyme does in an

https://dx.doi.org/10.1021/acs.joc.0c02519
J. Org. Chem. 2021, 86, 1701–1711

Table 1. Binding Data for MINPs Determined by ITC and Fluorescence Titration[a]

entry	host	guest (sodium salt of)	K_a ($\times 10^6$ M^{-1})	$-\Delta G$ (kcal/mol)	$-\Delta H$ (kcal/mol)	$T\Delta S$ (kcal/mol)	N[b]
1	MINP(**1a**)	**1a**	16.4 ± 4.2 (10.5 ± 7.44)	9.83	24.1 ± 0.45	−14.27	0.9 ± 0.01
2	MINP(**1a**)	**2a**	3.4 ± 0.3 (3.15 ± 0.35)	8.90	74.2 ± 1.47	−65.30	0.7 ± 0.01
3	MINP(**1a**)	**2b**	2.1 ± 0.2	8.61	23.1 ± 0.40	−14.48	1.4 ± 0.02
4	MINP(**1a**)	**2c**	0.068 ± 0.002 (0.070 ± 0.006)	6.59	1.6 ± 0.02	4.99	[c]
5	MINP(**1b**)	**1b**	2.5 ± 0.3 (2.43 ± 0.9)	8.72	45.9 ± 0.77	−37.18	1.2 ± 0.01
6	MINP(**1b**)	**2a**	<0.0004 ([d])	[c]	[c]	[c]	[c]
7	MINP(**1b**)	**2c**	0.9 ± 0.15 (1.03 ± 0.65)	8.12	1.0 ± 0.03	7.12	1.2 ± 0.02
8	MINP(**1b**)	**2d**	0.7 ± 0.04	7.97	3.6 ± 0.08	4.36	1.1 ± 0.02

[a]All the MINPs were prepared with a DVB/surfactant ratio of 0.5:1. Titrations were performed in duplicate using sodium salts of the templates and acid cofactors in 10 mM HEPES buffer (pH 7.0) with 2% DMSO. The errors between the runs were <10%. The binding constants in parentheses were obtained from fluorescence titration. [b]N is the number of binding sites per MINP determined by ITC. [c]Binding was extremely weak, and the binding constant was estimated from ITC. [d]Binding in the fluorescence titration was extremely weak, and the binding constant could not be obtained.

enzyme−cofactor complex, with the acid group pointing at the acetal oxygen for catalytic hydrolysis.

The preparation of the MINP started with spontaneous incorporation of the largely hydrophobic **1** into the micelle of surfactant **4**, together with 2,2-dimethoxy-2-phenyl acetophenone (DMPA, a photoinitiator) and various amounts of divinylbenzene (DVB). The tripropargylammonium headgroup of the surfactant allowed us to cross-link the surface of the micelle by diazide **5** and functionalize it with monoazide **6** by the Cu(I)-catalyzed click reaction. Molecular imprinting took place in the micellar core, when free-radical polymerization cross-linked the vinyl groups of DVB and the methacrylate of **4**, essentially to "solidify" the core around the template. Template removal happened during precipitation of the MINP from acetone and repeated solvent washing.[16] The synthesis of our templates **1a−d** is shown in Scheme 2.

Characterization of MINP Catalysts. The surface- and core-cross-linking of the micelle were monitored by ^{1}H NMR spectroscopy (Figure S1 in the Supporting Information). The size of the cross-linked micelle was determined by dynamic light scattering (DLS, Figures S2−S4), confirmed by transmission electron microscopy.[36] The formation of the imprinted site was studied by isothermal titration calorimetry (ITC), one of the most reliable methods to study intermolecular interactions.[37] A particular benefit of ITC is the simultaneous determination of binding enthalpy and binding free energy as well as the number of binding sites per nanoparticle (N) that could help us estimate the yield of micellar imprinting. For selected cases, we also confirmed the binding by fluorescence titration and found that the values obtained (shown in parentheses in Table 1) agreed well with those from ITC.

As shown in Table 1 (entry 1), MINP(**1a**) bound its template **1a** with a binding constant (K_a) of 16.4 × 10^6 M^{-1}, which translates to nearly 10 kcal/mol in binding free energy. In our preparation, a 50:1 surfactant/template ratio was used, and DLS indicated ∼50 cross-linked surfactants per nanoparticle (Supporting Information). The ideal yield of the imprinted site was thus an average of 1 binding site per nanoparticle. The number of binding sites determined by ITC was ∼0.9, suggesting a high yield in the formation and vacation of the imprinted sites.

MINP(**1a**) bound the sodium salts of pyrene acids **2a** and **2b** more weakly than its template **1a** by about 5−8 times (Table 1, entries 2−3)—the sodium salts had to be used because the acids were insoluble in water. The result was reasonable because the driving force in a hydrophobic binding process is directly proportional to the hydrophobic surface area buried upon binding.[38−40] The entire template was certainly larger than the acid cofactor which could only occupy a portion of the imprinted site.

MINP(**1a**) bound sodium 2-naphthalenecarboxylate (the conjugate base of **2c**) much more weakly than sodium 1-pyrenecarboxylate (the conjugate base of **2a**), by about 50 times (Table 1, entries 2 and 4). The result further supported successful imprinting, as the smaller naphthalene would not be able to fit fully inside the larger imprinted site created for the pyrenyl group of **1a**. Filling the unoccupied space of the hydrophobic imprinted site with water molecules was unfavorable.

When the binding between an MINP and its own template was compared, the K_a value was noticeably lower for MINP(**1b**) than for MINP(**1a**) (compare entries 1 and 5 of Table 1). This result was also expected from the hydrophobic binding that depended on the surface area of the host−guest interaction. Once again, the carboxylate salt of **2c** was bound more strongly than the sulfonate salt of **2d**, but the difference was not large (entries 7 and 8). Note that a mismatched but smaller cofactor (i.e., **2c**) could still enter the imprinted site of MINP(**1a**) (entry 4). For MINP(**1b**), the mismatched cofactor (i.e., **2a**) was not bound at all, apparently because of its larger size than the imprinted pocket (entry 6).

Validation of the Catalytic Design Hypothesis. Our ITC and fluorescence titration could only measure the binding of guests with some water solubility, including the templates and the sodium salts of the acid cofactors. The targeted substrate, 2-(4-nitrophenyl)-1,3-dioxolane (**3a**), was insoluble in water. Its binding by the MINP, nonetheless, was evident from the catalytic hydrolysis by the MINP-cofactor complex (Figure 1a). In the absence of MINP, **2a** was rather inactive under our experimental conditions (85 °C in D_2O) even at a concentration of 200 μM or 20 mol % of the substrate. With the matching MINP in the solution, both 1-pyrenecarboxylic acid (**2a**) and 2-naphthalenecarboxylic acid (**2c**) became active and could afford 45−61% yield under otherwise identical reaction conditions. The hydrolytic yield stabilized above a 1:1 cofactor/MINP ratio. For most of our experiments, we used a 2:1 ratio to ensure that the binding site of the MINP was saturated with the acid cofactor.

Figure 1b shows the hydrolysis of **3a** under different catalytic conditions as a function of solution pH. In the absence of MINP(**1a**), neither 1-pyrenecarboxylic acid (**2a**) nor 1-pyrenesulfonic acid (**2b**) showed any catalytic effect beyond

https://dx.doi.org/10.1021/acs.joc.0c02519
J. Org. Chem. 2021, 86, 1701−1711

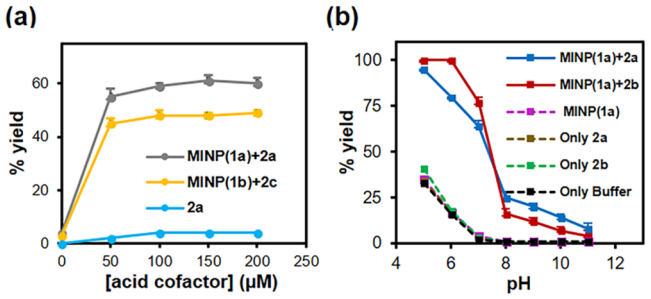

Figure 1. (a) Yield of hydrolysis for **3a** as a function of acid cofactor in D_2O at 85 °C under different conditions. Acid **2a** and **2c** were used with MINP(**1a**) and MINP(**1b**), respectively. The reaction without the MINP was performed with **2a**. (b) Hydrolysis of **3a** as a function of solution pH after 6 h at 85 °C under different catalytic conditions. Reactions were performed in duplicate with the yields determined by ^{1}H NMR spectroscopy using 1,4-dibromobenzene as an internal standard. [**3a**] = 1.0 mM. [MINP] = 50 μM. [**2a**] = [**2b**] = 100 μM. The MINPs were prepared with a DVB/surfactant ratio of 0.5:1.

that of the buffer and hydrolysis of the acetal was only observed below pH 7, consistent with the acid-catalyzed hydrolysis.[41] Once MINP(**1a**) was added, both **2a** and **2b** became quite effective in the hydrolysis. Even though the reaction slowed down at higher pH values, it was very impressive that the MINP-cofactor complex could perform an acid-catalyzed hydrolysis under basic conditions (pH 9−10), a feature rarely seen in synthetic catalysts.[8] By itself, MINP(**1a**) was also inactive, giving the same yields as the buffers.

The large drop in the hydrolytic yield over pH 6−8 suggests that a deprotonation occurred with the acid cofactor at higher pH values. The transition, however, was much larger than the pK_a of sulfonic acid (−7) or carboxylic acid (4−5).[42] It is known that the microenvironment around an acid or base can strongly impact its acidity/basicity, whether in the active site of an enzyme[43] or in a synthetic host.[44−46] For example, the ammonium side chain of a lysine has a pK_a of 10.6 in water but shifted to 5.6 in the active site of acetoacetate decarboxylase.

The two most common strategies to shift the pK_a of a functional group are through hydrophobic interactions[47] and ionic interactions.[48] The former takes advantage of the change of solvation during protonation or deprotonation. Because an ionic group is better solvated by polar solvents such as water, it becomes more difficult to protonate an amine or deprotonate a carboxylic acid when the functional group migrates into a hydrophobic microenvironment. A pK_a shift can also occur as a result of electrostatic interactions: vicinal positive charges generally make protonation more difficult and deprotonation easier.

Once these points are made clear, it is not a surprise to see that 1-pyrenecarboxylic acid (**2a**) and 1-pyrenesulfonic acid (**2b**) had their pK_a increased to ∼7 in Figure 1b. With a large hydrophobic group, these acid cofactors have a strong driving force to enter the matching hydrophobic binding site within MINP(**1a**). This hydrophobic effect (on the pK_a) apparently exceeded the electrostatic interactions of the ammonium head groups of the cross-linked surfactants that otherwise would decrease the pK_a of the acids.[49]

If the pK_a of 1-pyrenecarboxylic acid (**2a**) and 1-pyrenesulfonic acid (**2b**) indeed shifted to ∼7, the small degree of hydrolysis under basic conditions (up to pH 9−10) should be caused by the small amount of the protonated cofactor in the MINP binding site. The crossover between the two acid cofactors in Figure 1b (the blue and red lines) suggests a small advantage of the sulfonic acid over carboxylic acid at lower pH values but the opposite at higher pH values. According to the pH profiles, the reversal was a result of the more gradual transition seen in **2a**.

Encouraged by the abilities of the MINP to help the hydrolysis of **3a**, we performed additional structure−activity studies to understand the catalysis better and summarize the results in Table 2. A strong dependence of the catalysis on the

Table 2. Hydrolysis of 3a catalyzed by MINP-Acid Cofactor Complexes[a]

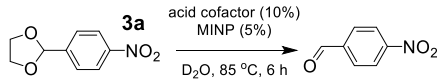

entry	MINP	DVB/4	acid cofactor	yield (%)
1	MINP(**1a**)	0	**2a**	23 ± 1
2	MINP(**1a**)	0.5	**2a**	59 ± 2
3	MINP(**1a**)	1	**2a**	42 ± 2
4	MINP(**1a**)	0	**2b**	33 ± 2
5	MINP(**1a**)	0.5	**2b**	71 ± 3
6	MINP(**1a**)	1	**2b**	57 ± 1
7	MINP(**1a**)	0.5	**2c**	29 ± 2
8	MINP(**1a**)	0.5	**2d**	37 ± 3
9	MINP(**1b**)	0.5	**2a**	3 ± 1
10	MINP(**1b**)	0.5	**2b**	4 ± 2
11	MINP(**1b**)	0.5	**2c**	48 ± 2
12	MINP(**1b**)	0.5	**2d**	64 ± 3
13	MINP(**1a**−**b**)	0.5	none	4 ± 1
14	none	-	**2a**−**d**	3 ± 2
15	NINP	0.5	none	3 ± 1
16	NINP	0.5	**2a**−**d**	5 ± 1
17	CTAB	-	**2a**	<5

[a]Reactions were performed in duplicate with the yields determined by ^{1}H NMR spectroscopy using 1,4-dibromobenzene as an internal standard. [**3a**] = 1.0 mM. [**2a**−**d**] = 100 μM. [MINP] = [NINP] = 50 μM. [CTAB] = 2.5 mM.

amount of DVB used in the MINP preparation was observed (entries 1−6). The micelle of **4** could solubilize up to 1 equiv of DVB relative to the surfactant. MINP(**1a**) prepared with DVB/surfactant = 0.5:1 was found to give a better yield than those with either no DVB or the maximum amount of DVB.

The rigidity of a cross-linked polymer such as MINP is determined by the cross-linking density. A large amount of DVB (the core cross-linker) is expected to increase the integrity of the polymer network and prevent the imprinted site from collapsing after the removal of the template. A smaller amount of DVB, on the other hand, should make the polymer network more flexible and can facilitate the binding and release of the substrate and product. The medium level of DVB apparently represented a good balance between the two.

We also performed several control experiments (Table 2, entries 13−16). MINP in the absence of an acid cofactor, the acid cofactors alone, the nonimprinted nanoparticle (NINP) by itself, or the cofactors in the presence of NINP showed negligible activity. These results demonstrate that the acid cofactor had to work together with the MINP to cause the hydrolysis, supporting our design hypothesis. The acid cofactor (**2a**) was not active in "normal" cationic micelles of cetyltrimethylammonium bromide (CTAB) (Table 2, entry 17). Apparently, the non-cross-linked micelle could not

https://dx.doi.org/10.1021/acs.joc.0c02519
J. Org. Chem. 2021, 86, 1701−1711

position the acid in the same way as our MINP that had the specific binding pockets for both the substrate and the acid cofactor.

Another support for the binding-induced catalysis was the proper matching between the imprinted pocket and the acid cofactor required for the hydrolysis. MINP(**1a**) had a pyrene-shaped pocket. With this MINP, the pyrenyl-based acids (**2a** or **2b**) gave a significantly higher yield in the hydrolysis than the smaller naphthyl-based acids (**2c** or **2d**) (Table 2, entries 2 and 5 vs 7 and 8). The results were in line with the binding data in Table 1, which showed a weaker but measurable binding for the smaller (sodium salt of) **2c**.

When MINP(**1b**) was used, the trend reversed, with the naphthyl-based acids (**2c** or **2d**) giving much higher yields than the pyrenyl-based acids (**2a** or **2b**) (Table 2, entries 9–12). In fact, the mismatched **2a** or **2b** was completely inactive, affording a yield similar to our negative controls. These results once again were in agreement with the ITC data that showed negligible binding between MINP(**1b**) and **2a** (Table 1) because of the larger size of the acids.

For both MINP(**1a**) and MINP(**1b**), sulfonic acids (**2b** and **2d**) were found to be more active than the corresponding carboxylic acids (**2a** and **2c**). Because the reaction was performed under neutral conditions, the trend was in line with the observation in Figure 1b.

Fine-Tuning of the Catalytic Active Site. The facile preparation of the MINP allowed us to tune the catalytic active site in multiple ways using readily synthesized template molecules. Template **1c** had a linear space holder for the acid cofactor. Our initial idea was to fine-tune the distance between the acid group and the acetal oxygen through acid cofactors **2e** and **2f** with different chain lengths. The chain length, however, made little difference in the hydrolysis (Table 3, entries 1 and 2).

Table 3. Hydrolysis of 3a catalyzed by MINP-Acid Cofactor Complexes[a]

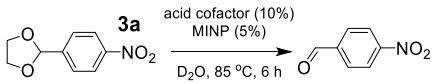

entry	MINP	DVB/4	acid cofactor	yield (%)
1	MINP(**1c**)	0.5	**2e**	68 ± 2
2	MINP(**1c**)	0.5	**2f**	65 ± 2
3	MINP(**1d**)	0.5	**2a**	77 ± 2
4	MINP(**1d**)	0.5	**2b**	86 ± 1
5	MINP(**1e**)	0.5	**2c**	83 ± 2
6	MINP(**1e**)	0.5	**2d**	84 ± 2
7	MINP(**1f**)	0.5	**2c**	80 ± 3
8	MINP(**1f**)	0.5	**2d**	81 ± 1

[a]Reactions were performed in duplicate with the yields determined by ^{1}H NMR spectroscopy using 1,4-dibromobenzene as an internal standard. [**3a**] = 1.0 mM. [**2a–f**] = 100 μM. [MINP] = 50 μM.

More interesting results were obtained when we prepared an MINP using template **1d**. This compound had a biphenyl-derived spacer holder for the substrate. Its linear framework, longer length in comparison to **1a**, and surface anchoring by the carboxylate were expected to produce a deeper active site, with the acid catalyst to be bound at the far end.

To our delight, the hydrolysis improved significantly as the active site became deeper. For example, 1-pyrenecarboxylic acid (**2a**) with MINP(**1a**) gave a 59% yield in the hydrolysis of **3a** at 85 °C after 6 h (Table 2, entry 2). The yield increased to 77% when MINP(**1d**) was used (Table 3, entry 3). The deeper pocket also helped 1-pyrenesulfonic acid (**2b**), increasing the yield from 71% to 86% (compare entry 5 of Table 2 and entry 4 of Table 3).

How could a deeper active site help the hydrolysis? Because binding was essential to the catalysis based on our earlier studies, we measured the binding constants of MINP(**1d**) for the acid cofactors (**2a** and **2b**). The numbers (Table 4, entries 2–3) turned out more than doubled those by MINP(**1a**) (Table 1, entries 2–3). We attributed the enhanced binding to a more hydrophobic binding pocket. The interfacial area of a micelle is significantly more polar than the nonpolar core because of increased water exposure. Moving the binding pocket deeper into the core should enhance its hydrophobicity.

In addition to changing the depth of the active site, we could also tune the number of acid cofactors using templates **1e** and **1f**, whose syntheses are shown in Schemes 3 and 4, respectively. We did not use a double-pyrenyl design here because too large a template could be trapped permanently inside a cross-linked micelle.[50] Of the two templates, **1e** matched substrate **3a** in structure better than **1f**, which had a 1,3-phenylene where the 1,3-dioxolane of the substrate was expected to reside.

Our ITC binding data indicated that micellar imprinting worked well for these templates as well. Both **1e** and **1f** were bound by their MINPs with a large binding constant, $>10^7$ M^{-1} (Table 4, entries 4 and 7). In addition, the binding data for the (sodium salts of the) acid cofactors fit well to a binding model with two sequential binding sites. The two bindings seemed independent as the binding constant was quite similar.

Most interestingly, even though the double-acid design improved the hydrolysis consistently, the improvement was much more pronounced with the weaker acid. The end result was that carboxylic acid **2c** became equally effective for the catalysis as sulfonic acid **2d**, with the two giving essentially the same yield (compare entries 5–8 of Table 3 with entries 11–12 of Table 2).

How could a carboxylic acid catalyze acetal hydrolysis as well as a much stronger sulfonic acid? Because this only happened in the double-acid catalyst, a simple answer could be a higher probability for both the carboxylic acids to stay protonated in the MINP-cofactor complex. When the acid becomes highly acidic, it might be quite difficult for the sulfonic acid cofactors to stay both protonated. If this is indeed the case, the benefit of having two catalytic groups would be lost.

Table 3 (entries 5–8) also showed that although **1e** seemed to give a slightly better yield than **1f**, the difference was statistically insignificant. This was good news because a perfect matching between the space holder and the substrate was not necessary.

These artificial enzyme–cofactor complexes displayed enzymelike kinetics. Figure 2 shows the Michaelis–Menten plot for MINP(**1e**) + **2c**, one of our most active catalysts. Nonlinear least-squares curve fitting yielded a V_{max} value of 0.45 ± 0.02 μM/min, a K_m of 389 ± 52 μM, and a k_{cat} of 22.6 × 10^{-3} min^{-1}. The catalytic efficiency (k_{cat}/K_m) was 57.9 M^{-1} min^{-1}.

Substrate Selectivity of MINP Catalysts. With a specifically shaped active site, our MINP should hydrolyze acetals in a selective manner. For this purpose, we used MINP(**1d**), with a deeper substrate binding site, to hydrolyze a

https://dx.doi.org/10.1021/acs.joc.0c02519
J. Org. Chem. 2021, 86, 1701–1711

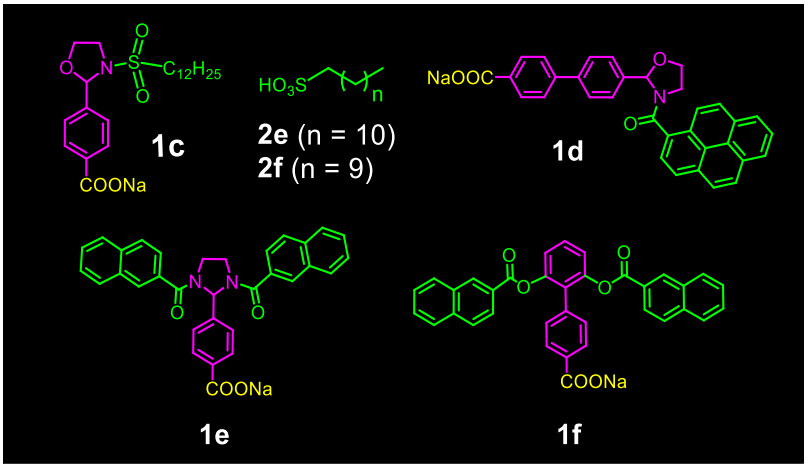

Table 4. Binding Data for MINPs Determined by ITC and Fluorescence Titration[a]

entry	host	guest (sodium salt of)	K_a ($\times 10^6$ M^{-1})	$-\Delta G$ (kcal/mol)	$-\Delta H$ (kcal/mol)	$T\Delta S$ (kcal/mol)	N[b]
1	MINP(**1d**)	**1d**	105 ± 25 (108 ± 60)	10.93	26.9 ± 0.27	−15.97	0.8 ± 0.003
2	MINP(**1d**)	**2a**	8.8 ± 0.45 (9.08 ± 0.22)	9.47	189.6 ± 1.35	−180.14	0.7 ± 0.004
3	MINP(**1d**)	**2b**	6.0 ± 0.25	9.24	39.9 ± 0.16	−30.66	1.4 ± 0.004
4	MINP(**1e**)	**1e**	11.2 ± 0.6	9.61	96.8 ± 0.45	−87.19	1.2 ± 0.003
5	MINP(**1e**)	**2c**	0.17 ± 0.02 and 0.41 ± 0.04	7.13 & 7.65	39.8 ± 2.4 and 6.90 ± 2.58	−32.7 and 0.75	2[c]
6	MINP(**1e**)	**2d**	0.11 ± 0.01 and 0.22 ± 0.01	6.87 & 7.28	44.1 ± 2.0 and 64.2 ± 2.6	−37.2 and −56.9	2[c]
7	MINP(**1f**)	**1f**	24.1 ± 5.2	10.06	49.0 ± 0.8	−38.94	0.9 ± 0.01
8	MINP(**1f**)	**2c**	0.64 ± 0.09 and 0.51 ± 0.04	7.91 & 7.78	50.8 ± 1.4 and 62.7 ± 2.0	−42.9 and −54.9	2[c]
9	MINP(**1f**)	**2d**	0.47 ± 0.12 and 0.42 ± 0.09	7.73 & 7.66	54.8 ± 4.0 and 4.35 ± 4.68	−47.07 and 3.32	2[c]

[a]All the MINPs were prepared with a DVB/surfactant ratio of 0.5:1. Titrations were performed in duplicate using sodium salts of the templates and acid cofactors in 10 mM HEPES buffer (pH 7.0) with 2% DMSO. The errors between the runs were <10%. The binding constants in parentheses were obtained from fluorescence titration. [b]N is the number of binding sites per MINP determined by ITC. [c]Titration data were fitted to a binding model with two sequential binding sites.

Scheme 3. Synthesis of Compound 1e

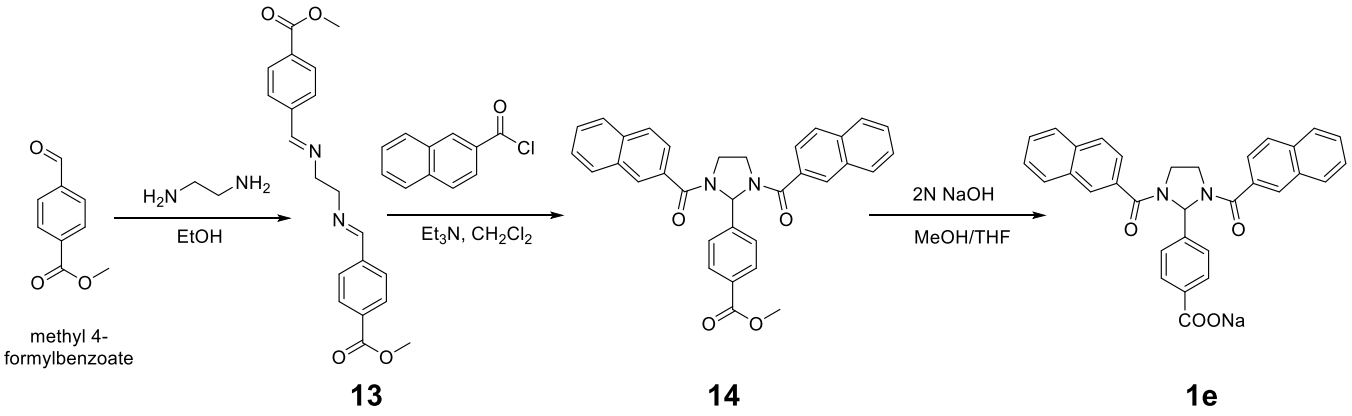

number of acetal analogues to understand the selectivity. Although the double-acid MINPs showed comparable activities (Table 3), we did not use them because some of the substrates (e.g., **3e**) were expected to enter the naphthalene-shaped pockets for the acid cofactors. Also, the binding energy between acid cofactor **2a** and MINP(**1d**) was extremely large (Table 4, entry 2 for the sodium salt). This was another important factor to consider. Hydrophobic interactions are nonspecific by itself, and the binding selectivity comes from the size/shape complementarity. When a large pyrene cofactor was present, it would be difficult for the substrates (**3a**−**g**) to compete with the cofactor for the pyrene-shaped binding site.

For the selectivity experiments, because these acetals had different intrinsic reactivity, we kept the reaction time at 6 h but varied the temperature so that the background hydrolysis stayed relatively slow during the reaction time. As shown in Table 2, the background hydrolysis could be estimated from the hydrolytic yields obtained in the presence of MINP or the acid cofactor alone.

Table 5 shows that MINP(**1d**) + **2a** could hydrolyze **3b** and **3c** quite well. If the ratio of the catalyzed yield over that of the background was used to estimate the catalytic efficiency, the order was **3a** > **3b** > **3c**. Thus, all the para-substituted benzaldehyde acetals were reasonable substrates for the MINP catalyst, and the one with the lowest intrinsic activity benefited

https://dx.doi.org/10.1021/acs.joc.0c02519
J. Org. Chem. 2021, 86, 1701−1711

Scheme 4. Synthesis of Compound 1f

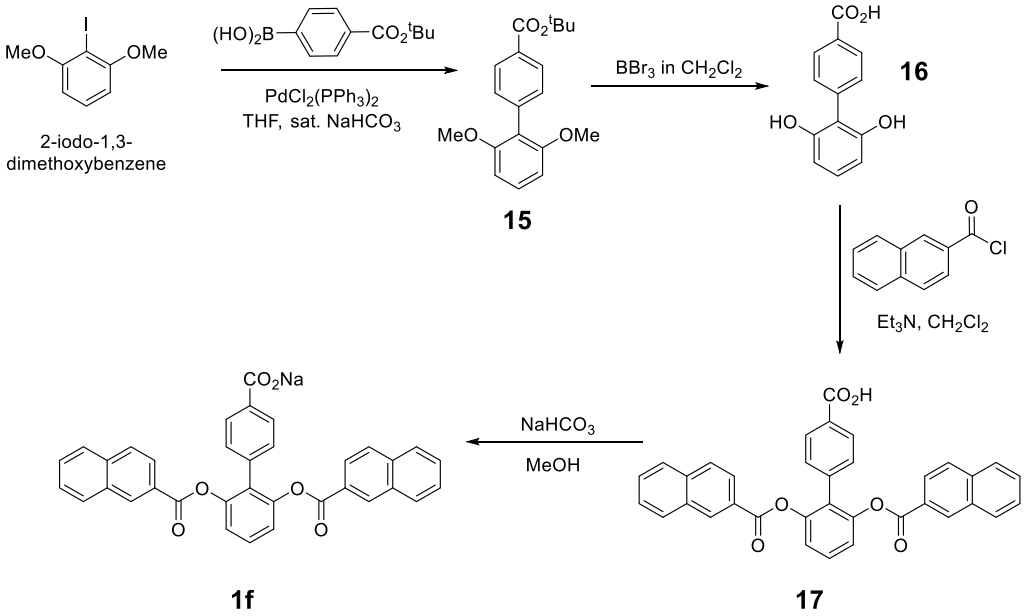

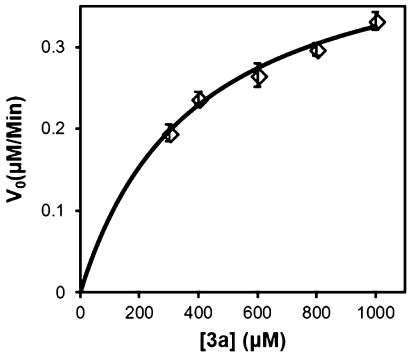

Figure 2. Michaelis–Menten plot for the hydrolysis of **3a** by MINP(**1e**) + **2c**. The reaction rates were measured in D_2O at 85 °C. [MINP(**1e**)] = 20 μM. [**2c**] = 40 μM. Reaction progress was monitored by ^1H NMR spectroscopy using 1,4-dibromobenzene as an internal standard. The MINPs were prepared with a DVB/surfactant ratio of 0.5:1.

the most from the catalysis. For the two naphthyl acetals **3d** and **3e**, the 2-naphthyl derivative was a much better substrate than the 1-naphthyl one, even though their background reactivity was similar. The most likely reason for the selectivity should be their different shape, with **3e** bearing a higher resemblance to **3a**, the substrate that the catalyst was designed for.

The most interesting selectivity was found in **3f** and **3g**. Diethyl acetal **3f** is known to hydrolyze faster than 1,3-dioxolane acetal **3a** by over 20 times in solution.[41] However, when catalyzed by MINP(**1d**) + **2a**, **3f** hydrolyzed very little (Table 5), while **3a** hydrolyzed easily under identical conditions (Table 3). The long and narrow pocket generated from **1d** thus seemed to have difficulty accommodating the acyclic acetals **3f** and **3g** or at least was poorly suited for catalysis.

One might wonder that, if large guests such as **2a** or **2b** could get into the far end of the imprinted site within MINP(**1d**) according to ITC (Table 4), the active site for the substrate must be able to "breathe" to let relatively large molecules to pass through. In this case, why did not **3f** or **3g** do the same to get in and be converted? In our opinion, this indeed could happen given the overall flexibility of the cross-linked structure, as depicted in Scheme 1. Nonetheless, once **2a** occupies the catalytic site, even if **3f** or **3g** could get into the active site, their residence time, position, and/or orientation within the active site must not be right for the catalysis to happen.

CONCLUSIONS

Enzymes have inspired generations of chemists with their fascinating performance. Difficulty in the construction of complex-shaped active sites with accurately positioned catalytic groups continues to hamper our design and synthesis of enzyme mimics. This work demonstrates that with micellar imprinting, one can quickly construct a substrate-tailored nanospace in a water-soluble protein-sized organic nanoparticle, with catalytic groups positioned near the reactive functionality. The size/shape selectivity of the imprinted site allowed the substrate and the acid cofactor each to occupy its designed position—an extremely important feature of our system.

Nature uses unimpressive functional groups for challenging catalysis, but chemists often have to resort to strong acids and expensive metals not available in a biological system. The stronger performance of a deeper active site in our catalytic hydrolysis was a useful learning, which could provide guidance to the design of future artificial enzymes. MINP(**1e**/**f**) demonstrated that with a proper design of the active site, weak carboxylic acids could become as effective as stronger sulfonic acids.

Overall, our method made modulation of the catalytic activity readily achievable through systematic tuning of the active site. The resulting artificial enzyme was able to override intrinsic reactivity of substrates, a feature frequently found in enzymes but difficult to obtain with synthetic catalysts. As a cross-linked polymeric nanoparticle, MINP tolerates high temperature, organic solvents,[51] and extreme pH.[52] These features plus the facile construction and modification of the

https://dx.doi.org/10.1021/acs.joc.0c02519
J. Org. Chem. 2021, 86, 1701–1711

Table 5. Hydrolytic Yields of Acetal Analogues by MINP Catalysts[a]

	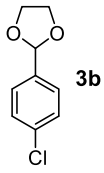 3b	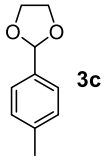 3c	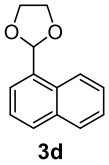 3d
MINP(**1d**)+**2a**	100%	100%	23%
MINP(**1d**)	18%	23%	18%
2a	16%	20%	14%
reaction conditions	50 °C for 6 h	25 °C for 6 h	85 °C for 6 h

	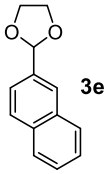 3e	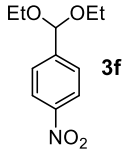 3f	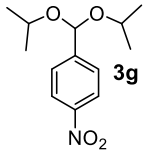 3g
MINP(**1d**)+**2a**	73%	10%	14%
MINP(**1d**)	20%	7%	8%
2a	15%	6%	5%
reaction conditions	85 °C for 6 h	85 °C for 6 h	85 °C for 6 h

[a][acetal] = 1.0 mM. [**2a**] = 100 μM. [MINP(**1d**)] = 50 μM. The MINPs were prepared with a DVB/surfactant ratio of 0.5:1.

active site make it a very versatile platform for artificial enzymes.

EXPERIMENTAL SECTION

General Experimental Methods. All organic solvents and reagents were of ACS-certified grade or higher grade and were purchased from commercial suppliers. Chemicals shifts are reported in parts per million (ppm) relative to residual solvent peaks. Coupling constants are reported in hertz. Electrospray ionization−high-resolution mass spectrometry (ESI-HRMS) was performed on an Agilent QTOF 6540 mass spectrometer with a QTOF detector. Milli-Q water (18.2 MU; Millipore Co., USA) was used for MINP preparation and all buffers. DLS data were obtained on a Malvern Zetasizer Nano ZS at 25 °C. ITC was performed using a MicroCal VP-ITC Microcalorimeter with Origin 7 software and VPViewer2000 (GE Healthcare, Northampton, MA). Fluorescence spectra were recorded at ambient temperature on a Varian Cary Eclipse Fluorescence spectrophotometer.

Syntheses of substrates **3a**−**c**/**f**,[35] **3d**,[53] surfactant **4**,[54] cross-linker **5**,[16] surface ligand **6**,[16] **7**,[55] and **13**[35] were reported previously. Syntheses of substrates **3e**[56] and **3g**[57] were adapted from the known procedures.

Compound ***8***. A solution of methyl 4′-formyl-[1,1′-biphenyl]-4-carboxylate (1.2 g, 5 mmol, 1.0 equiv) and 2-aminoethanol (0.32 mL, 5.25 mmol, 1.05 equiv) in toluene (80 mL) was heated to reflux in an oil bath with a Dean−Stark apparatus to remove water for 7 h. After the solvent was removed by rotary evaporation, the residue was used directly in the next step without further purification. A white powder (1.10 g, 81%). ^{1}H NMR (400 MHz, DMSO-d_6): δ 8.37 (s, 1H), 8.05−8.03 (m, 2H), 7.88−7.85 (m, 4H), 7.83−7.81 (m, 2H), 4.63 (t, J = 4 Hz, 1H), 3.86 (s, 3H), 3.68−3.66 (m, 4H) ppm. ^{13}C{^{1}H} NMR (100 MHz, DMSO-d_6): δ 166.0, 161.2, 143.9, 140.6, 136.1, 129.9, 128.7, 128.6, 127.2, 127.0, 63.4, 60.7, 52.2. HRMS (ESI) m/z: [M + H]$^+$ calcd for $C_{17}H_{17}NO_3$, 284.1281; found, 284.1274.

General Procedure for the Synthesis of Compounds 9−12. Pyridine (10 mmol, 2.0 equiv) was added to a solution of the appropriate acid chloride (3.85 mmol, 0.77 equiv) and compound **7** or **8** (5 mmol, 1.0 equiv) in ethyl acetate (40 mL). The reaction mixture was stirred at 50 °C in an oil bath for 6 h. After the mixture was cooled to room temperature, the solid precipitate was removed by filtration and the solvents were removed by rotary evaporation. The residue was purified by flash chromatography over silica gel using 15:1 dichloromethane/ethyl acetate as the eluent to afford the final product.

Compound ***9***. A white powder (0.68 g, 41%). ^{1}H NMR (400 MHz, $CDCl_3$): δ 8.19−7.42 (bm, 13H), 6.82−6.71 (m, 1H), 4.48−3.24 (m, 7H). ^{13}C{^{1}H} NMR (100 MHz, $CDCl_3$): δ 169.5, 166.7, 143.8, 132.1, 130.9, 130.5, 130.5, 129.9, 129.1, 128.5, 128.4, 127.4, 126.9, 126.8, 126.4, 126.2, 125.9, 125.7, 124.5, 124.2, 124.1, 123.5, 88.5, 66.5, 52.1, 47.2. HRMS (ESI) m/z: [M + H]$^+$ calcd for $C_{28}H_{21}NO_4$, 436.1543; found, 436.1542.

Compound ***10***. A white powder (1.18 g, 85%). ^{1}H NMR (400 MHz, $CDCl_3$): δ 8.12−7.36 (m, 11H), 6.85−6.72 (m, 1H), 4.40−3.34 (m, 7H). ^{13}C{^{1}H} NMR (100 MHz, $CDCl_3$): δ 168.9, 166.7, 143.7, 133.8, 130.4, 130.0, 129.8, 129.3, 129.2, 128.5, 127.3, 126.7, 126.5, 126.5, 124.9, 124.5, 88.3, 66.5, 52.1, 47.1. HRMS (ESI) m/z: [M + H]$^+$ calcd for $C_{22}H_{19}NO_4$, 362.1387; found, 362.1391.

Compound ***11***. A white powder (1.37 g, 70%). ^{1}H NMR (400 MHz, $CDCl_3$): δ 8.26−7.70 (m, 15H), 6.85−6.67 (m, 3H), 4.55−3.38 (m, 7H). ^{13}C{^{1}H} NMR (100 MHz, $CDCl_3$): δ 169.5, 167.0, 145.2, 140.6, 138.9, 132.3, 131.2, 130.8, 130.2, 129.8, 129.2, 128.7, 128.4, 127.6, 127.5, 127.2, 127.0, 126.7, 126.5, 126.3, 126.1, 125.8, 124.7, 124.3, 124.2, 123.8, 89.1, 66.6, 52.2, 47.5. HRMS (ESI) m/z: [M + H]$^+$ calcd for $C_{34}H_{25}NO_4$, 512.1856; found, 512.1858.

https://dx.doi.org/10.1021/acs.joc.0c02519
J. Org. Chem. 2021, 86, 1701−1711

Compound ***12***. A white powder (0.56 g, 33%). ^{1}H NMR (400 MHz, $CDCl_3$): δ 7.97 (d, J = 8.4 Hz, 2H), 7.51 (d, J = 8.4 Hz, 2H), 6.23 (s, 1H), 4.07−3.92 (m, 2H), 3.85 (s, 3H), 3.81−3.75 (m, 1H), 3.34−3.29 (m, 1H), 2.88−2.84 (m, 2H), 1.76−1.71 (m, 2H), 1.31−1.17 (m, 18H), 0.80 (t, J = 6.4 Hz, 3H). ^{13}C{^{1}H} NMR (100 MHz, $CDCl_3$): δ 166.6, 142.9, 130.7, 129.8, 126.7, 90.1, 66.0, 52.2, 51.4, 46.2, 31.9, 29.6, 29.5, 29.4, 29.3, 29.3, 29.1, 28.4, 23.0, 22.7, 14.2. HRMS (ESI) m/z: $[M + H]^+$ calcd for $C_{23}H_{37}NO_5S$, 440.2465; found, 440.2465.

General Procedure for the Synthesis of Compounds 1a−d. The appropriate ester (**9**−**12**, 0.5 mmol, 1.0 equiv) was dissolved in a 2:1 methanol/ tetrahydrofuran (THF) mixture (2 mL), to which 1 mL of aqueous NaOH solution (2 N) was added. The reaction mixture was stirred at room temperature for 5 h, followed by the addition of 2 mmol of sodium bicarbonate. After 10 min, the insoluble solid was removed by filtration and the solvents were removed by rotary evaporation. The residue was purified by flash chromatography over silica gel using 1:5 methanol/dichloromethane as the eluent to afford the final product.

Compound ***1a***. A white powder (0.21 g, 93%). ^{1}H NMR (400 MHz, DMSO-d_6): δ 13.05 (br s, 1H), 8.50−7.40 (bm, 13H), 6.87−6.60 (m, 1H), 4.35−3.30 (m, 4H). ^{13}C{^{1}H} NMR (100 MHz, DMSO-d_6): δ 167.9, 167.2, 143.9, 139.4, 131.5, 131.1, 130.7, 130.1, 129.8, 129.5, 128.8, 128.4, 127.8, 127.1, 126.9, 126.4, 126.1, 125.8, 124.8, 124.5, 123.8, 123.7, 88.7, 66.3, 47.4. HRMS (ESI) m/z: $[M + H]^+$ calcd for $C_{27}H_{19}NO_4$, 422.1387; found, 422.1391.

Compound ***1b***. A white powder (0.18 g, 97%). ^{1}H NMR (400 MHz, DMSO-d_6): δ 13.00 (br s, 1H), 8.17−7.15 (m, 10H), 6.92−6.90 (m, 1H), 6.51 (s, 1H), 4.21−3.57 (m, 4H). ^{13}C{^{1}H} NMR (100 MHz, DMSO-d_6): δ 167.6, 167.1, 143.9, 134.1, 133.1, 131.1, 129.7, 129.5, 128.8, 128.5, 127.3, 127.2, 126.9, 126.5, 125.3, 124.6, 88.3, 66.4, 47.2. HRMS (ESI) m/z: $[M + H]^+$ calcd for $C_{21}H_{17}NO_4$, 348.1230; found, 348.1229.

Compound ***1d***. A white powder (0.21 g, 80%). ^{1}H NMR (400 MHz, DMSO-d_6): δ 12.98 (br s, 1H), 8.38−7.71 (m, 15H), 7.00−6.58 (m, 3H), 4.35−3.32 (m, 4H). ^{13}C{^{1}H} NMR (100 MHz, DMSO-d_6): δ 167.9, 167.2, 143.9, 139.5, 131.6, 131.2, 130.7, 130.2, 130.1, 129.5, 128.8, 128.5, 127.8, 127.3, 127.1, 126.9, 126.9, 126.8, 126.5, 126.1, 125.9, 125.6, 124.9, 124.5, 123.8, 123.7, 88.8, 66.3, 47.5. HRMS (ESI) m/z: $[M + H]^+$ calcd for $C_{33}H_{23}NO_4$, 498.1700; found, 498.1701.

Compound ***1c***. A white powder (0.08 g, 34%). ^{1}H NMR (400 MHz, $CDCl_3$): δ 8.13 (d, J = 8.4 Hz, 2H), 7.63 (d, J = 8.4 Hz, 2H), 6.33 (s, 1H), 4.16−4.00 (m, 2H), 3.90−3.81 (m, 1H), 3.44−3.35 (m, 1H), 2.99−2.90 (m, 2H), 1.87−1.77 (m, 2H), 1.45−1.15 (m, 18H), 0.87 (t, J = 6.8 Hz, 3H). ^{13}C{^{1}H} NMR (100 MHz, $CDCl_3$): δ 171.2, 144.0, 130.6, 129.9, 126.9, 110.1, 90.2, 66.2, 51.6, 46.3, 32.1, 29.7, 29.6, 29.5, 29.4, 29.2, 28.5, 23.1, 22.8, 14.3. HRMS (ESI) m/z: $[M - H]^-$ calcd for $C_{22}H_{35}NO_5S$, 424.2163; found, 424.2172.

Compound ***14***. 2-Naphthoyl chloride (1.08 g, 5.68 mmol, 4.0 equiv) in dry dichloromethane (15 mL) was slowly added to a solution of **13** (0.50 g, 1.42 mmol, 1.0 equiv) and triethylamine (0.79 mL, 5.68 mmol, 4.0 equiv) in dry dichloromethane (15 mL) at 0 °C under nitrogen. The reaction mixture was warmed to room temperature and stirred for 12 h. After the mixture was washed with saturated $NaHCO_3$, brine, and dried (Na_2SO_4), the solvent was removed by rotary evaporation. The residue was purified by column chromatography over silica gel using 1:1 hexane/ethyl acetate as the eluent to give an orange powder (0.55 g, 76%). ^{1}H NMR (600 MHz, DMSO-d_6): δ 9.00−8.78 (m, 2H), 8.53−8.45 (m, 2H), 8.02−7.95 (m, 10H), 7.75 (d, J = 6.0 Hz, 1H), 7.63−7.57 (m, 4H), 3.87−3.51 (m, 7H). ^{13}C{^{1}H} NMR (100 Hz, DMSO-d_6): δ 166.6, 165.8, 137.3, 134.2, 134.1, 131.9, 131.2, 130.3, 129.9, 129.4, 128.8, 127.8, 127.6, 127.5, 126.7, 124.2, 52.3, 49.5, 46.4. HRMS (ESI) m/z: $[M + H]^+$ calcd for $C_{33}H_{26}N_2O_4$, 515.1971; found, 515.1959.

Compound ***1e***. Compound **14** (0.20 g, 0.39 mmol, 1.0 equiv) was dissolved in a 2:1 methanol/THF mixture (2 mL), to which 1 mL of aqueous NaOH solution (2 N) was added. The reaction mixture was stirred at room temperature for 5 h, followed by the addition of sodium bicarbonate (0.17 g, 2.0 mmol, 5.13 equiv). After 10 min, the insoluble solid was removed by filtration and the solvents were removed by rotary evaporation. The residue was purified by flash chromatography over silica gel using 1:5 methanol/dichloromethane as the eluent to afford an orange powder (0.18 g, 91%). ^{1}H NMR (400 MHz, DMSO-d_6): δ 8.53−8.42 (m, 2H), 8.38−8.21 (m, 2H), 8.19−7.57 (m, 9H), 7.54−7.03 (m, 6H), 3.49−3.17 (m, 4H). ^{13}C{^{1}H} NMR (100 MHz, 323 K, DMSO-d_6): δ 170.6, 166.9, 142.0, 138.2, 137.6, 133.2, 132.5, 128.8, 128.4, 128.1, 127.2, 126.5, 126.3, 125.7, 125.5, 125.4, 125.0, 45.3. HRMS (ESI) m/z: $[M - H]^-$ calcd for $C_{32}H_{24}N_2O_4$, 499.1663; found, 499.1655.

Compound ***15***. A mixture of (4-(*tert*-butoxycarbonyl)phenyl)-boronic acid (0.15 g, 0.70 mmol, 1.67 equiv), 2-iodo-1,3-dimethoxybenzene (0.11 g, 0.42 mmol, 1.0 equiv), and bis-(triphenylphosphine)palladium(II) chloride (0.05 g, 0.07 mmol, 0.17 equiv) in dry THF (20 mL) and saturated $NaHCO_3$ solution (25 mL) was heated at 70 °C in an oil bath under nitrogen overnight. The organic solvent was removed by rotary evaporation, and the aqueous solution was extracted with dichloromethane (3 × 30 mL). The combined organic solution was washed with brine (3 × 20 mL) and dried over Na_2SO_4 and filtered. Dichloromethane was removed by rotary evaporation, and the residue was purified by column chromatography over silica gel using 1:5 ethyl acetate/hexane as the eluent to give a white powder (0.08 g, 62%). ^{1}H NMR (400 MHz, $CDCl_3$): δ 8.06 (d, J = 8.0 Hz, 2H), 7.42 (d, J = 8.0 Hz, 2H), 7.32 (t, J = 8.0 Hz, 1H), 6.67 (d, J = 8.0 Hz, 2H), 3.74 (s, 6H), 1.63 (s, 9H). ^{13}C{^{1}H} NMR (100 MHz, $CDCl_3$): δ 165.9, 157.6, 139.0, 131.0, 130.4, 129.3, 128.9, 118.8, 104.3, 80.7, 55.9, 28.4. HRMS (ESI) m/z: $[M + H]^+$ calcd for $C_{19}H_{22}O_4$, 315.1591; found, 315.1571.

Compound ***16***. 1 mL of BBr_3 in dry dichloromethane (1 M) was slowly added to a solution of **15** (0.10 g, 0.32 mmol, 1.0 equiv) in dry dichloromethane (30 mL) at −78 °C. The reaction mixture was warmed to room temperature and stirred for 15 h. After the reaction was complete, the mixture was cooled to 0 °C and quenched by the dropwise addition of water, followed by acidification with HCl (2 N), and the organic phase was separated. The aqueous phase was extracted with EtOAc (3 × 20 mL). The combined organic layers were dried over Na_2SO_4, filtered, and removed by rotary evaporation. The residue was purified over silica gel using 2:5 ethyl acetate/hexane as the eluent to give a white powder (0.05 g, 68%). ^{1}H NMR (400 MHz, CD_3OD): δ 8.02 (d, J = 8.0 Hz, 2H), 7.49 (d, J = 8.0 Hz, 2H), 6.97 (t, J = 8.0 Hz, 1H), 6.42 (d, J = 8.0 Hz, 2H). ^{13}C{^{1}H} NMR (100 MHz, CD_3OD): δ 170.2, 156.6, 141.7, 132.4, 130.1, 129.9, 129.6, 117.0, 108.2. HRMS (ESI) m/z: $[M - H]^-$ calcd for $C_{13}H_{10}O_4$, 229.0506; found, 229.0503.

Compound ***17***. 2-Naphthoyl chloride (0.18 g, 0.95 mmol, 2.2 equiv) in dry dichloromethane (10 mL) was slowly added to a solution of **16** (0.10 g, 0.43 mmol, 1.0 equiv) and triethylamine (0.13 mL, 0.95 mmol, 2.2 equiv) in dry dichloromethane (10 mL) at 0 °C under nitrogen. The reaction mixture was warmed to room temperature and stirred for 16 h. After the mixture was washed with saturated $NaHCO_3$, brine, and dried (Na_2SO_4), the solvent was removed by rotary evaporation. The residue was purified by column chromatography over silica gel using 5:1 hexane/ethyl acetate as the eluent to give an orange powder (0.14 g, 61%). ^{1}H NMR (600 MHz, $CDCl_3$): δ 8.46 (s, 2H), 7.91−7.82 (m, 9H), 7.60−7.53 (m, 8H), 7.37 (d, J = 8.0 Hz, 2H). ^{13}C{^{1}H} NMR (150 MHz, $CDCl_3$): δ 166.8, 164.9, 149.4, 137.4, 135.9, 132.5, 132.1, 131.2, 130.1, 129.6, 129.5, 129.4, 128.8, 128.5, 127.9, 126.9, 126.8, 126.2, 125.3, 120.9. HRMS (ESI) m/z: $[M - H]^-$ calcd for $C_{35}H_{22}O_6$, 537.1344; found, 537.1337.

Compound ***1f***. Compound **17** (0.10 g, 0.18 mmol, 1.0 equiv) and sodium bicarbonate (0.017 g, 0.20 mmol, 1.1 equiv) were dissolved in 10 mL of methanol, and the reaction mixture was stirred overnight at room temperature. After the reaction mixture was concentrated by rotary evaporation, the residual white powder (0.09 g, 89%) was used in MINP preparation without further purification.

Preparation of MINP. A typical procedure is as follows: to a micellar solution of surfactant **4** (10.2 mg, 0.02 mmol) in H_2O (2.0 mL) were added DVB (2.8 μL, 0.02 mmol), DMPA in DMSO (10 μL of a 12.8 mg/mL solution, 0.0005 mmol), and the relative template in

https://dx.doi.org/10.1021/acs.joc.0c02519
J. Org. Chem. 2021, 86, 1701−1711

DMSO (10 μL of a 0.04 M solution, 0.0004 mmol). The mixture was subjected to ultrasonication for 10 min before cross-linker **5** (4.1 mg, 0.024 mmol), $CuCl_2$ in H_2O (10 μL of 6.7 mg/mL solution, 0.0005 mmol), and sodium ascorbate in H_2O (10 μL of 99 mg/mL solution, 0.005 mmol) were added. After the reaction mixture was stirred slowly at room temperature for 12 h, compound **6** (15.9 mg, 0.06 mmol), $CuCl_2$ in H_2O (10 μL of 6.7 mg/mL solution, 0.0005 mmol), and sodium ascorbate in H_2O (10 μL of 99 mg/mL solution, 0.005 mmol) were added. The mixture was stirred at room temperature for another 6 h, purged with nitrogen for 15 min, sealed with a rubber stopper, and irradiated in a Rayonet reactor for 12 h. The reaction mixture was then poured into acetone (8 mL). The precipitate was collected by centrifugation and washed with a mixture of acetone/water (5 mL/1 mL) three times, followed by methanol/acetic acid (5 mL/0.1 mL) three times. The solid was then rinsed twice with acetone (5 mL) and dried in air to afford the final MINPs as an off-white powder. Typical yields were >80%.

Determination of Binding Constants by ITC. In general, a solution of an appropriate guest in 10 mM *N*-(2-hydroxyethyl)-piperazine-*N*′-ethanesulfonic acid (HEPES) buffer (pH 7.0) with 2% DMSO at 298 K (DMSO was added to help the solubility of the appropriate guest) was injected in equal steps into 1.43 mL of the corresponding MINP in the same solution. The top panel shows the raw calorimetric data. The area under each peak represents the amount of heat generated at each ejection and is plotted against the molar ratio of the MINP to the guest. The solid line is the best fit of the experimental data to the sequential binding of *N* equal and independent binding sites on the MINP. The heat of dilution for the substrate, obtained by adding the substrate to the buffer, was subtracted from the heat released during the binding. Binding parameters were autogenerated after curve fitting using Microcal Origin 7. All titrations were performed in duplicate, and the errors between the runs were <10% using sodium salts of the templates and acid cofactors.

Catalytic Hydrolysis of Acetals with MINPs. A typical procedure is as follows: a 4.0 μL aliquot of the acid cofactor (**2a**−**f**) in DMSO-d_6 (0.025 M) was added to an MINP solution (2.5 mg in 991 μL of D_2O), and the mixture was sonicated for 5 min. A 5.0 μL aliquot of substrate **3a** in DMSO-d_6 (0.20 M) was added, and the reaction mixture was kept at 85 °C for 6 h in a block heater. After the reaction mixture was cooled to room temperature, it was extracted with 600 μL of $CDCl_3$. The organic phase was dried by Na_2SO_4, and a 500 μL portion of the organic phase was transferred into an NMR tube, followed by the addition of 1,4-dibromobenzene in DMSO-d_6 as the internal standard. The reaction yield was determined by ^{1}H NMR spectroscopy.

Catalytic Hydrolysis of Acetals with CTAB. A typical procedure is as follows: an aliquot of the acid cofactor (**2a**) in DMSO-d_6 (0.025 M) was added to a CTAB solution (2.5 mM) in 1 mL of D_2O, and the mixture was sonicated for 5 min. A 5.0 μL aliquot of substrate **3a** in DMSO-d_6 (0.20 M) was added, and the reaction mixture was kept at 85 °C in a block heater. After the reaction mixture was cooled to room temperature, it was transferred into an NMR tube, followed by the addition of 1,4-dibromobenzene in DMSO-d_6 as the internal standard. The reaction yield was determined by ^{1}H NMR spectroscopy.

■ ASSOCIATED CONTENT

Supporting Information

The Supporting Information is available free of charge at https://pubs.acs.org/doi/10.1021/acs.joc.0c02519.

Characterization of MINPs, ITC and fluorescence titration curves, and NMR spectra of key compounds (PDF)

■ AUTHOR INFORMATION

Corresponding Author

Yan Zhao − *Department of Chemistry, Iowa State University, Ames, Iowa 50011-3111, United States;* orcid.org/0000-0003-1215-2565; Email: zhaoy@iastate.edu

Authors

Ishani Bose − *Department of Chemistry, Iowa State University, Ames, Iowa 50011-3111, United States*

Shixin Fa − *Department of Chemistry, Iowa State University, Ames, Iowa 50011-3111, United States*

Complete contact information is available at: https://pubs.acs.org/10.1021/acs.joc.0c02519

Notes

The authors declare no competing financial interest.

■ ACKNOWLEDGMENTS

We thank the NIGMS (R01GM138427) for financial support of this research.

■ REFERENCES

(1) Jencks, W. P. *Catalysis in Chemistry and Enzymology*; Dover: New York, 1987.

(2) Hedstrom, L. Serine Protease Mechanism and Specificity. *Chem. Rev.* **2002**, *102*, 4501−4524.

(3) Dunn, B. M. Structure and Mechanism of the Pepsin-Like Family of Aspartic Peptidases. *Chem. Rev.* **2002**, *102*, 4431−4458.

(4) Lairson, L. L.; Withers, S. G. Mechanistic analogies amongst carbohydrate modifying enzymes. *Chem. Commun.* **2004**, 2243−2248.

(5) Zechel, D. L.; Withers, S. G. Glycosidase mechanisms: Anatomy of a finely tuned catalyst. *Acc. Chem. Res.* **2000**, *33*, 11−18.

(6) Das, S.; Incarvito, C. D.; Crabtree, R. H.; Brudvig, G. W. Molecular Recognition in the Selective Oxygenation of Saturated C-H Bonds by a Dimanganese Catalyst. *Science* **2006**, *312*, 1941−1943.

(7) Yoshizawa, M.; Tamura, M.; Fujita, M. Diels-Alder in Aqueous Molecular Hosts: Unusual Regioselectivity and Efficient Catalysis. *Science* **2006**, *312*, 251−254.

(8) Pluth, M. D.; Bergman, R. G.; Raymond, K. N. Acid Catalysis in Basic Solution: A Supramolecular Host Promotes Orthoformate Hydrolysis. *Science* **2007**, *316*, 85−88.

(9) Shugrue, C. R.; Miller, S. J. Applications of Nonenzymatic Catalysts to the Alteration of Natural Products. *Chem. Rev.* **2017**, *117*, 11894−11951.

(10) Cho, H.; Zhong, Z.; Zhao, Y. A DMAP-functionalized oligocholate foldamer for solvent-responsive catalysis. *Tetrahedron* **2009**, *65*, 7311−7316.

(11) Chadha, G.; Zhao, Y. Environmental control of nucleophilic catalysis in water. *Chem. Commun.* **2014**, *50*, 2718−2720.

(12) Lee, L.-C.; Zhao, Y. Metalloenzyme-Mimicking Supramolecular Catalyst for Highly Active and Selective Intramolecular Alkyne Carboxylation. *J. Am. Chem. Soc.* **2014**, *136*, 5579−5582.

(13) Lee, L.-C.; Xing, X.; Zhao, Y. Environmental Engineering of Pd Nanoparticle Catalysts for Catalytic Hydrogenation of CO_2 and Bicarbonate. *ACS Appl. Mater. Interfaces* **2017**, *9*, 38436−38444.

(14) Haupt, K.; Mosbach, K. Molecularly Imprinted Polymers and Their Use in Biomimetic Sensors. *Chem. Rev.* **2000**, *100*, 2495−2504.

(15) Wulff, G. Molecular Imprinting in Cross-Linked Materials with the Aid of Molecular Templates—A Way towards Artificial Antibodies. *Angew. Chem., Int. Ed. Engl.* **1995**, *34*, 1812−1832.

(16) Awino, J. K.; Zhao, Y. Protein-Mimetic, Molecularly Imprinted Nanoparticles for Selective Binding of Bile Salt Derivatives in Water. *J. Am. Chem. Soc.* **2013**, *135*, 12552−12555.

(17) Wulff, G. Enzyme-like Catalysis by Molecularly Imprinted Polymers. *Chem. Rev.* **2002**, *102*, 1−28.

(18) Wulff, G.; Liu, J. Design of biomimetic catalysts by molecular imprinting in synthetic polymers: the role of transition state stabilization. *Acc. Chem. Res.* **2012**, *45*, 239−247.
(19) Sellergren, B.; Karmalkar, R. N.; Shea, K. J. Enantioselective Ester Hydrolysis Catalyzed by Imprinted Polymers. 2§,‖. *J. Org. Chem.* **2000**, *65*, 4009−4027.
(20) Emgenbroich, M.; Wulff, G. A New Enzyme Model For Enantioselective Esterases Based On Molecularly Imprinted Polymers. *Chem.—Eur. J.* **2003**, *9*, 4106−4117.
(21) Liu, J.-q.; Wulff, G. Functional Mimicry of Carboxypeptidase A by a Combination of Transition State Stabilization and a Defined Orientation of Catalytic Moieties in Molecularly Imprinted Polymers. *J. Am. Chem. Soc.* **2008**, *130*, 8044−8054.
(22) Kirsch, N.; Hedin-Dahlström, J.; Henschel, H.; Whitcombe, M. J.; Wikman, S.; Nicholls, I. A. Molecularly imprinted polymer catalysis of a Diels-Alder reaction. *J. Mol. Catal. B: Enzym.* **2009**, *58*, 110−117.
(23) Chen, Z. Y.; Xu, L.; Liang, Y.; Zhao, M. P. pH-Sensitive Water-Soluble Nanospheric Imprinted Hydrogels Prepared as Horseradish Peroxidase Mimetic Enzymes. *Adv. Mater.* **2010**, *22*, 1488−1492.
(24) Servant, A.; Haupt, K.; Resmini, M. Tuning Molecular Recognition in Water-Soluble Nanogels with Enzyme-Like Activity for the Kemp Elimination. *Chem.—Eur. J.* **2011**, *17*, 11052−11059.
(25) Muratsugu, S.; Tada, M. Molecularly Imprinted Ru Complex Catalysts Integrated on Oxide Surfaces. *Acc. Chem. Res.* **2013**, *46*, 300−311.
(26) Shen, X.; Huang, C.; Shinde, S.; Jagadeesan, K. K.; Ekström, S.; Fritz, E.; Sellergren, B. Catalytic Formation of Disulfide Bonds in Peptides by Molecularly Imprinted Microgels at Oil/Water Interfaces. *ACS Appl. Mater. Interfaces* **2016**, *8*, 30484−30491.
(27) Zheng, A.-x.; Gong, C.-b.; Zhang, W.-j.; Tang, Q.; Huang, H.-r.; Chow, C.-f.; Tang, Q. An amphiphilic and photoswitchable organocatalyst for the aldol reaction based on a product-imprinted polymer. *Mol. Catal.* **2017**, *442*, 115−125.
(28) Wei, W.; Zhou, T.; Wu, S.; Shen, X.; Zhu, M.; Li, S. An enzyme-like imprinted-polymer reactor with segregated quantum confinements for a tandem catalyst. *RSC Adv.* **2018**, *8*, 1610−1620.
(29) Yuan, Y.; Yang, Y.; Faheem, M.; Zou, X.; Ma, X.; Wang, Z.; Meng, Q.; Wang, L.; Zhao, S.; Zhu, G. Molecularly Imprinted Porous Aromatic Frameworks Serving as Porous Artificial Enzymes. *Adv. Mater.* **2018**, *30*, 1800069.
(30) Muratsugu, S.; Shirai, S.; Tada, M. Recent progress in molecularly imprinted approach for catalysis. *Tetrahedron Lett.* **2020**, *61*, 151603.
(31) Chen, K.; Zhao, Y. Effects of nano-confinement and conformational mobility on molecular imprinting of cross-linked micelles. *Org. Biomol. Chem.* **2019**, *17*, 8611−8617.
(32) Zangiabadi, M.; Zhao, Y. Selective Binding of Complex Glycans and Glycoproteins in Water by Molecularly Imprinted Nanoparticles. *Nano Lett.* **2020**, *20*, 5106−5110.
(33) Duan, L.; Zangiabadi, M.; Zhao, Y. Synthetic lectins for selective binding of glycoproteins in water. *Chem. Commun.* **2020**, *56*, 10199−10202.
(34) Zangiabadi, M.; Zhao, Y. Molecularly Imprinted Polymeric Receptors with Interfacial Hydrogen Bonds for Peptide Recognition in Water. *ACS Appl. Polym. Mater.* **2020**, *2*, 3171−3180.
(35) Bose, I.; Zhao, Y. pH-Controlled Nanoparticle Catalysts for Highly Selective Tandem Henry Reaction from Mixtures. *ACS Catal.* **2020**, *10*, 13973−13977.
(36) Fa, S.; Zhao, Y. Peptide-Binding Nanoparticle Materials with Tailored Recognition Sites for Basic Peptides. *Chem. Mater.* **2017**, *29*, 9284−9291.
(37) Schmidtchen, F. P. Isothermal Titration Calorimetry in Supramolecular Chemistry. In *Supramolecular Chemistry: From Molecules to Nanomaterials*; Steed, J. W., Gale, P. A., Eds.; Wiley: Weinheim, 2012.
(38) Tanford, C. *The Hydrophobic Effect: Formation of Micelles and Biological Membranes*, 2nd ed.; Krieger: Malabar, Florida, 1991.
(39) Ben-Naim, A., *Hydrophobic Interactions*; Plenum Press: New York, 1980.
(40) Southall, N. T.; Dill, K. A.; Haymet, A. D. J. A view of the hydrophobic effect. *J. Phys. Chem. B* **2002**, *106*, 521−533.
(41) Fife, T. H.; Jao, L. K. Substituent Effects in Acetal Hydrolysis. *J. Org. Chem.* **1965**, *30*, 1492−1495.
(42) Smith, M.; March, J. *March's Advanced Organic Chemistry: Reactions, Mechanisms, and Structure*, 8th ed.; John Wiley & Sons, Incorporated: Hoboken, New Jersey, 2020.
(43) Westheimer, F. H. Coincidences, decarboxylation, and electrostatic effects. *Tetrahedron* **1995**, *51*, 3−20.
(44) Marquez, C.; Nau, W. M. Two Mechanisms of Slow Host−Guest Complexation between Cucurbit[6]uril and Cyclohexylmethylamine: pH-Responsive Supramolecular Kinetics. *Angew. Chem., Int. Ed.* **2001**, *40*, 3155−3160.
(45) Bakirci, H.; Koner, A. L.; Schwarzlose, T.; Nau, W. M. Analysis of Host-Assisted Guest Protonation Exemplified for p-Sulfonatocalix[4]arene—Towards Enzyme-Mimetic pK_a Shifts. *Chem. —Eur. J.* **2006**, *12*, 4799−4807.
(46) Widanapathirana, L.; Zhao, Y. Tuning Nanopore Formation of Oligocholate Macrocycles by Carboxylic Acid Dimerization in Lipid Membranes. *J. Org. Chem.* **2013**, *78*, 4610−4614.
(47) Matulis, D.; Bloomfield, V. A. Thermodynamics of the hydrophobic effect. I. Coupling of aggregation and pK_a shifts in solutions of aliphatic amines. *Biophys. Chem.* **2001**, *93*, 37−51.
(48) Henao, J. D.; Suh, Y.-W.; Lee, J.-K.; Kung, M. C.; Kung, H. H. Striking Confinement Effect: $AuCl_4^-$ Binding to Amines in a Nanocage Cavity. *J. Am. Chem. Soc.* **2008**, *130*, 16142−16143.
(49) Electrostatic repulsion of the ammonium headgroups was not as important as the hydrophobic effect, possibly because there was a significant distance between the acid cofactor and the ammoniums on the surface of the micelle (Scheme 1).
(50) Zhang, S.; Zhao, Y. Artificial metalloenzymes via encapsulation of hydrophobic transition-metal catalysts in surface-crosslinked micelles (SCMs). *Chem. Commun.* **2012**, *48*, 9998−10000.
(51) Xing, X.; Zhao, Y. Binding-promoted chemical reaction in the nanospace of a binding site: effects of environmental constriction. *Org. Biomol. Chem.* **2018**, *16*, 2855−2859.
(52) Xing, X.; Zhao, Y. Fluorescent nanoparticle sensors with tailor-made recognition units and proximate fluorescent reporter groups. *New J. Chem.* **2018**, *42*, 9377−9380.
(53) Müller, P.; Nury, P.; Bernardinelli, G. Asymmetric Nucleophilic Substitution of Acetals. *Eur. J. Org. Chem.* **2001**, *2001*, 4137−4147.
(54) Arifuzzaman, M.; Zhao, Y. Water-Soluble Molecularly Imprinted Nanoparticle Receptors with Hydrogen-Bond-Assisted Hydrophobic Binding. *J. Org. Chem.* **2016**, *81*, 7518−7526.
(55) Ling, Y.; Feng, J.; Luo, L.; Guo, J.; Peng, Y.; Wang, T.; Ge, X.; Xu, Q.; Wang, X.; Dai, H.; Zhang, Y. Design and Synthesis of C3-Substituted *β*-Carboline-Based Histone Deacetylase Inhibitors with Potent Antitumor Activities. *ChemMedChem* **2017**, *12*, 646−651.
(56) Hassner, A.; Bandi, C.; Panchgalle, S. A Mild, Room-Temperature Protection of Ketones and Aldehydes as 1,3-Dioxolanes under Basic Conditions. *Synlett* **2012**, *23*, 2773−2776.
(57) Huo, C.; Chan, T. H. Carbon Tetrabromide/Sodium Triphenylphosphine-m-sulfonate (TPPMS) as an Efficient and Easily Recoverable Catalyst for Acetalization and Tetrahydropyranylation Reactions. *Adv. Synth. Catal.* **2009**, *351*, 1933−1938.

https://dx.doi.org/10.1021/acs.joc.0c02519
J. Org. Chem. 2021, 86, 1701−1711